View metadata, citation and similar papers at core.ac.uk
brought to you by CORE
provided by Gunma University Academic Information Repository

JOURNAL OF APPLIED PHYSICS VOLUME 96, NUMBER 6 15 SEPTEMBER 2004

Optical properties of N^+ ion-implanted and rapid thermally annealed Si(100) wafers studied by spectroscopic ellipsometry

Katsunori Kurihara, Shin-ichi Hikino, and Sadao Adachi[a)]
Department of Electronic Engineering, Faculty of Engineering, Gunma University, Kiryu-shi, Gunma 376-8515, Japan

(Received 9 April 2004; accepted 7 June 2004)

The optical properties of N^+ ion-implanted Si(100) wafers have been studied using the spectroscopic ellipsometry (SE). The N^+ ions are implanted at 150 keV with fluences in the range between 1×10^{16} and 7.5×10^{16} cm^{-2} at room temperature. A Bruggeman effective-medium-approximation and a linear-regression analysis require a four-phase model (substrate/first and second damaged layers/ambient) to explain the experimental data of the as-implanted samples. These analyses suggest that the buried fully amorphous layer can be formed at around $\sim 5\times 10^{16}$ cm^{-2} dose. The rapid thermal annealing is performed at 750 °C in a dry N_2 atmosphere on N^+ ion-implanted samples. The SE data reveal that the recrystallization starts to occur very quickly. The time constant for the defect annealing in the deeper damaged layer is determined to be 36 s. The dielectric-function spectra $\varepsilon(E)$ of microcrystalline silicon deduced here differ appreciably from that of the single-crystalline silicon, especially in the vicinity of the critical points. © *2004 American Institute of Physics*. [DOI: 10.1063/1.1777807]

I. INTRODUCTION

Nitrogen is an interesting impurity in silicon. It locks the dislocations and leads to the hardening of the single-crystalline silicon.[1] The formation of the buried dielectric layer by nitrogen ion implantation has been reported for the realization of various silicon-on-insulator devices. Typically, high-fluences ($\sim 10^{17}$ cm^{-2}) and high-temperature ($\geqslant$1000 °C) annealing have been required for this purpose.[2,3] Furthermore, it has been reported that an *n*-type conductivity can be associated with the lower nitrogen ($10^{14}-10^{16}$ cm^{-2}) implants following low-temperature annealing at 700–900 °C, but that the doping efficiency at ~1% is too low to be of practical consequences.[4]

As a result of the accumulation of the radiation damage, the amorphized layer can be built up by the ion implantation on crystalline substance.[5] The actual processes of such amorphization have been studied in detail by the cross-section transmission electron microscopy, by the Rutherford backscattering, or by the other related surface-analytical techniques.[6–9] Most of these techniques require extensive and time-consuming sample preparations that often destroy the integrity of the microelectronic device fabrication. The spectroscopic ellipsometry (SE) has, however, the advantage that it is nondestructive and does not require any special sample preparation. Therefore, it has been used recently by many authors to characterize the amorphized silicon layers produced by energetic ions, such as H^+,[10] He^+,[11] B^+,[12] C^+,[13] Si^+,[14–16] P^+,[12,17] Ar^+,[8,9,18] Ge^+,[19] As^+,[12,20,21] and Xe^+.[18]

The usual way of describing the optical properties of such damaged layers is to assume that the layers consist of a physical mixture of crystalline and amorphous components in order to use an effective-medium approximation (EMA).[22] Although a better understanding has been gained in the area of the ion-implantation technology, nothing or not very much is known about the damaged layers produced by the N^+ ion implantation into silicon substrates.

In this article, we study the optical properties of Si(100) wafers implanted with N^+ ions at 175 eV. In order to extract the qualitative and the quantitative information on the ion-implanted layers, we use the Bruggeman EMA[22] assuming that the partially amorphized layer is a mixture of fully amorphous (*a*-) and crystalline silicon (*c*-Si). The results on the rapid thermal annealing of N^+ ion-implanted samples are also presented. Here, the annealed layer is assumed to be microcrystalline silicon (μc-Si) and its optical properties are deduced from a simplified model of the interband transitions, named, the model dielectric function (MDF; see Appendix). The best values of the structural parameters are determined from the liner regression analysis (LRA).[23]

II. EXPERIMENTAL METHOD

The N^+ ion implantation was made on Si(100) wafers at 150 keV for several doses from 1×10^{16} to 7.5×10^{16} cm^{-2}. The wafers were tilted 7° away from the main crystal axis so as to reduce the channeling effect. During the implantation, the substrate holder was cooled at approximately room temperature by flowing cold water (17 °C). To obtain a good thermal contact, silicone rubber was inserted between the substrate holder and the cold water. After the implantation, the highest-dose (7.5×10^{16} cm^{-2}) wafer was cut into a number of smaller specimens and was subjected to the isothermal-annealing experiments. Annealing was carried out at 750 °C in a dry N_2 atmosphere using a rapid thermal annealer for the time period between 40 and 90 s. The rapid thermal annealer used here was of the near-infrared lamp type (MILA3000-P-N, ULVAC-RIKO).

[a)]Electronic mail: adachi@el.gunma-u.ac.jp

 © 2004 American Institute of Physics

Downloaded 11 Oct 2007 to 210.151.113.98. Redistribution subject to AIP license or copyright, see http://jap.aip.org/jap/copyright.jsp

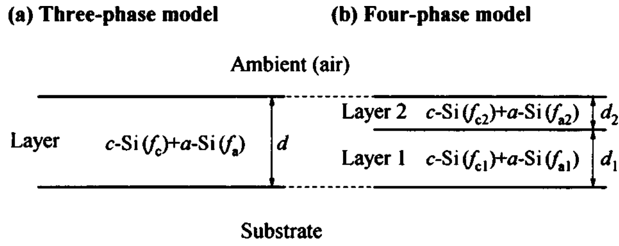

FIG. 1. (a) Three-phase and (b) four-phase models used in the Bruggeman EMA–LRA program.

The automatic ellipsometer was of the polarizer-sample-rotating-analyzer type (DVA-36VW-A, Mizojiri Optical). A 150 W xenon lamp was used as a light source. After cleaning the sample surfaces using organic solvents, they were etched in a 1.5% aqueous HF solution to remove the native oxide layer. The SE measurements were then carried out in the 1.2–5.2 eV photon-energy range at room temperature. The angle of the incidence and the polarizer azimuth were set at 70° and 30°, respectively.

III. ANALYTICAL MODEL

The Bruggeman EMA is used to analyze the optical properties of N^+ ion-implanted Si(100) wafers. It can be defined by the following two expressions:[22]

$$\sum_{i=1}^{n} f_i \frac{\varepsilon_i - \varepsilon}{\varepsilon_i + 2\varepsilon} = 0, \tag{1}$$

$$\sum_{i=1}^{n} f_i = 1, \tag{2}$$

where f_i and ε_i are, respectively, the volume fraction and the complex dielectric function of each of the components i (c-Si or a-Si) and ε is the complex dielectric function of the ion-implanted damaged layer.

The measured SE data are analyzed on the basis of Fresnel's reflection coefficients using a multiphase model. We show in Fig. 1 the three-phase and the four-phase models considered in the present analysis. The Fresnel's reflection coefficient in the jth layer ($j=0$: substrate) can now be written as

$$R_j = \frac{r_{j+1} + R_{j-1} e^{-i2\delta_j}}{1 + r_{j+1} R_{j-1} e^{-i2\delta_j}}, \tag{3}$$

with

$$R_0 = r_1, \tag{4}$$

$$r_j = \frac{n_{j-1} - n_j}{n_{j-1} + n_j}, \tag{5}$$

$$\delta_j = \frac{2\pi}{\lambda} n_j d_j \cos \phi_j, \tag{6}$$

where n_j is the refractive index in the jth layer, λ is the light wavelength in the vacuum, d_j is the thickness of the jth layer, and ϕ_j is the incident angle at the $j/(j-1)$th interface. The optical constants at each layer can be determined by measuring the complex reflectivity R for both s- and p-polarized light at fixed angle ϕ.

The dielectric function of unknown layer or unknown parameters such as layer thickness and volume fractions of constituent phases can be determined by minimizing the following mean squares deviation using the LRA program[23]

$$\sigma^2 = \frac{1}{N-P-1} \sum_{j=1}^{N} [(\tan \Psi_j^{\text{exp}} - \tan \Psi_j^{\text{calc}})^2 + (\cos \Delta_j^{\text{exp}} - \cos \Delta_j^{\text{calc}})^2], \tag{7}$$

where N is the number of data points and P is the number of unknown model parameters. The Ψ and the Δ are the ratio of amplitudes and the difference in phase of reflectance for s- and p-polarized light, respectively. A best-fit model is selected, which yields a minimum value of unbiased estimator σ.

The $\varepsilon(E)$ spectra for c-Si, a-Si, and μc-Si are modeled by means of the MDF calculation. Note that the MDF was developed for the calculation of the optical constants of crystalline substrates.[24] It has, however, been shown recently that the optical response of amorphous semiconductors can also be represented by the MDF well.[25] This approach is justified by the fact that the short-range order is important to understand the optical properties of both crystalline and amorphous semiconductors. Because the critical points (CP's) do not have any validity in amorphous material, the band gaps used in the MDF are not a result of the Bragg gaps at the Brillouin-zone boundaries but are considered to arise from the short-range order determined by the covalent bonding. With this success, we can calculate the optical properties of not only perfectly crystalline but also fully amorphous material using the common basis, namely, the MDF.

IV. RESULTS AND DISCUSSION

A. As-implanted samples

Figure 2 shows the real and the imaginary parts of the pseudodielectric function, $\varepsilon(E)=\varepsilon_1(E)+i\varepsilon_2(E)$, for N^+ ion-implanted Si(100) wafers with various ion fluences. For comparison, the $\varepsilon(E)$ spectrum of unimplanted Si(100) wafer (c-Si) is also shown by the solid circles. The oscillations observed in the lower spectral region ($E \leqslant 2$ eV) originated from multiple reflections in the N^+ ion-implanted layer.

In Fig. 2, we can identify at least two CP's in the measured $\varepsilon(E)$ spectrum of c-Si. The vertical arrows indicate the positions of these CP's (E_1 and E_2). They arise from singularities in the joint density of states.[26,27] A single-broad peak observed in the $\varepsilon_2(E)$ spectra for samples implanted with $\geqslant 4.5 \times 10^{16}$ cm^{-2} is a typical behavior of amorphous tetrahedrally bonded semiconductors. The disappearance of CP features in a-Si is due to the breakdown of lattice periodicity (i.e., a lack of the long-range ordering).

The dielectric behavior of the N^+ ion-implanted wafers is substantially different from that of the unimplanted sample. In order to present more qualitative and quantitative information on these spectral differences, we performed the Bruggeman EMA–LRA based on the multilayer structures shown in Fig. 1.

Downloaded 11 Oct 2007 to 210.151.113.98. Redistribution subject to AIP license or copyright, see http://jap.aip.org/jap/copyright.jsp

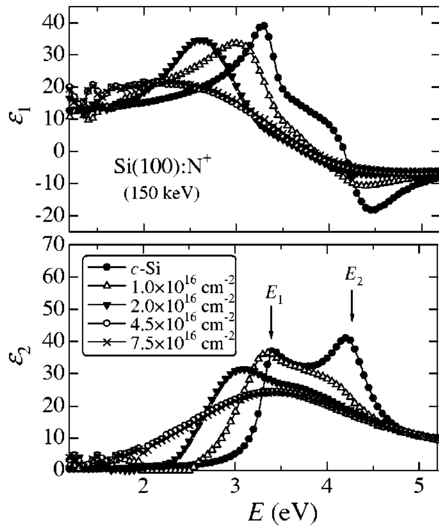

FIG. 2. Dielectric-function spectra, $\varepsilon(E)=\varepsilon_1(E)+i\varepsilon_2(E)$, for N^+ ion-implanted Si(100) at 150 keV with doses from 1×10^{16} to 7.5×10^{16} cm^{-2}, together with that for c-Si. The vertical arrows indicate the positions of several CP's (E_1 and E_2).

TABLE I. Brugemman EMA–LRA parameters obtained from the four-phase model in Fig. 1 for N^+ ion-implanted Si(100) with various ion fluences.

Fluences (cm^{-2})	Parameter	Layer 1	Layer 2	σ
Unimpla. (c-Si)	d(Å)	4400	—	0.005 3
	f_c(%)	100	—	
	f_a(%)	0	—	
1×10^{16}	d(Å)	4340	60	0.023 8
	f_c(%)	99	21	
	f_a(%)	1	79	
2×10^{16}	d(Å)	4291	109	0.020 8
	f_c(%)	91	9	
	f_a(%)	9	91	
4.5×10^{16}	d(Å)	4190	210	0.008 4
	f_c(%)	12	1	
	f_a(%)	88	99	
7.5×10^{16} (a-Si)	d(Å)	4400	—	0.008 8
	f_c(%)	0	—	
	f_a(%)	100	—	

Figure 3 shows the Bruggeman EMA–LRA results for the samples implanted with 1×10^{16} cm^{-2} and 7.5×10^{16} cm^{-2}, together with that for c-Si. The results assuming the four-phase model are shown by the solid lines. The structural parameters obtained here are summarized in Table I. The corresponding σ values are listed in the last column of Table I. The c-Si and a-Si $\varepsilon(E)$ spectra used as references in the Bruggeman EMA analysis are the same as those shown in Figs. 3(a) and 3(c) by the solid lines, respectively. They are obtained from the sum of Eqs. (A1), (A3), (A4), and (A6) in the Appendix. The CP parameters used for c-Si and a-Si are listed in Table II. The dashed lines in Fig. 3(b) indicate the calculated results assuming the three-phase model. It is understood from Fig. 3(b) that the optical properties of the crystalline/amorphous intermediate states can be interpreted by the four-phase model very well.

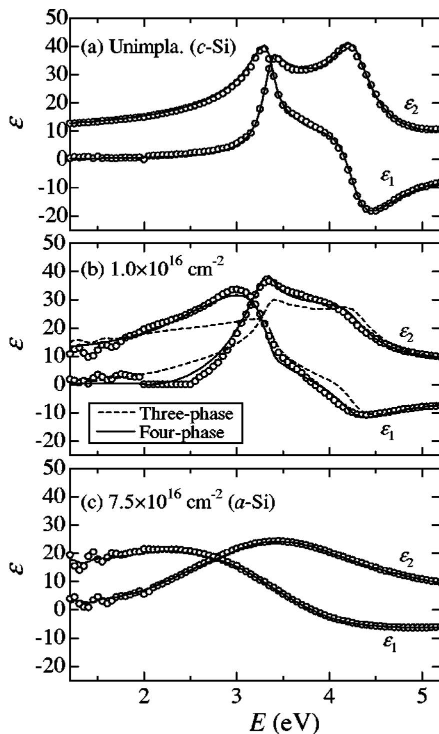

FIG. 3. Bruggeman EMA–LRA results for N^+ ion-implanted Si(1000) at 150 keV with 1×10^{16} cm^{-2} and 7.5×10^{16} cm^{-2}, together with that for c-Si. The SE data are indicated by the open circles, whereas the simulated results using the four-phase model are shown by the solid lines. The results of the three-phase model are also shown in (b) by the dashed lines.

As expected, the modeled interference pattern is dependent on the damaged layer thickness $d(=d_1+d_2)$. We obtained good agreement with the experimental data with $d\sim4400$ Å. The transport of ions in matter (TRIM) calculation predicts the damaged layer thickness of ~4500 Å. Our obtained d value is in good agreement with this TRIM calculation.

Figure 4 plots the amorphous fraction f_{a1} in Layer 1, obtained from the four-phase model, as a function of ion fluence $[N^+]$. From this plot, we obtain the relationship between f_{a1} and $[N^+]$ (in cm^{-2}) written as

$$f_a=\left(\frac{[N^+]}{A}\right)^{\alpha}, \tag{8}$$

where $A=4.7\times10^{16}$ cm^{-2} is an amorphization threshold fluence (i.e., minimum fluence required to form fully amorphous layer) and the exponent $\alpha=2.77$ is an amorphization rate factor. The straight line in Fig. 4 shows the calculated result of Eq. (8). It is noted that the crystalline target can be more efficiently amorphized by heavy ions than by light ions. It is, thus, expected that the threshold fluence A may be larger for lighter ions than for heavier ones. In fact, our obtained A value for N^+ ions (4.7×10^{16} cm^{-2}) is considerably larger than that for Si^+ ions (1.4×10^{15} cm^{-2}) (Ref. 16).

B. Rapid thermal annealing

Figure 5 shows the SE $\varepsilon(E)$ spectra for N^+ ion-implanted Si(100) annealed at 750 °C for six different times, $t=40, 50, 60, 70, 80$, and 90 s. For comparison, the $\varepsilon(E)$ spectra for c-Si and as-implanted sample ($t=0$ s; a-Si) are shown by the heavy and the light solid lines, respectively. As seen in

Downloaded 11 Oct 2007 to 210.151.113.98. Redistribution subject to AIP license or copyright, see http://jap.aip.org/jap/copyright.jsp

TABLE II. MDF parameters used in the calculation of $\varepsilon(E)$ for μc-Si produced by isothermal annealing at 750 °C for t=40–90 s. The values without and within the parentheses correspond to those in Layers 1 and 2 (Fig. 1), respectively. The second and the third columns correspond to those for a perfectly crystalline (c-Si) and a fully amorphous (t=0 s) material, respectively. The damaged layer thickness d and the LRA parameter σ are also shown in the last two rows.

			Annealing time					
Parameter	c-Si	a-Si	40 s	50 s	60 s	70 s	80 s	90 s
E_1 (eV)	3.37	2.95	3.08	3.10	3.16	3.25	3.27	3.29
			(3.16)	(3.16)	(3.20)	(3.29)	(3.31)	(3.33)
B_1	5.10	5.35	5.27	5.26	5.22	5.17	5.16	5.15
			(5.22)	(5.22)	(5.20)	(5.15)	(5.14)	(5.12)
B_{1x} (eV^2)	11.8	1.76	4.80	5.30	6.80	8.80	9.30	9.80
			(6.80)	(6.80)	(7.80)	(9.80)	(10.3)	(10.8)
Γ (eV)	0.113	0.420	0.328	0.313	0.266	0.205	0.189	0.174
			(0.266)	(0.266)	(0.235)	(0.174)	(0.158)	(0.144)
E_2 (eV)	4.27	4.00	4.08	4.10	4.14	4.19	4.20	4.22
			(4.14)	(4.14)	(4.16)	(4.22)	(4.23)	(4.24)
C	2.60	3.2	3.02	2.99	2.9	2.78	2.75	2.72
			(2.9)	(2.9)	(2.84)	(2.72)	(2.69)	(2.66)
Γ	0.114	0.550	0.420	0.398	0.332	0.244	0.223	0.201
			(0.332)	(0.332)	(0.288)	(0.201)	(0.179)	(0.157)
F	4.34	4.27	4.29	4.29	4.31	4.32	4.32	4.33
			(4.31)	(4.31)	(4.31)	(4.33)	(4.33)	(4.33)
Γ (eV)	0.108	0.560	0.423	0.40	0.333	0.243	0.221	0.196
			(0.333)	(0.333)	(0.288)	(0.196)	(0.176)	(0.153)
E_0' (eV)	3.35	2.60	2.83	2.87	2.98	3.13	3.16	3.20
			(2.98)	(2.98)	(3.05)	(3.20)	(3.23)	(3.28)
C	0.30	2.50	1.84	1.73	1.39	0.95	0.84	0.73
			(1.39)	(1.39)	(1.17)	(0.73)	(0.62)	(0.52)
γ	0.15	0.43	0.35	0.33	0.29	0.23	0.22	0.21
			(0.29)	(0.29)	(0.26)	(0.21)	(0.19)	(0.18)
E_1' (eV)	5.32	4.90	5.03	5.05	5.11	5.19	5.22	5.24
			(5.11)	(5.11)	(5.15)	(5.24)	(5.26)	(5.28)
C	0.20	0.30	0.27	0.27	0.25	0.23	0.23	0.22
			(0.25)	(0.25)	(0.24)	(0.22)	(0.22)	(0.21)
γ	0.09	0.30	0.24	0.23	0.19	0.15	0.14	0.13
			(0.19)	(0.19)	(0.17)	(0.13)	(0.12)	(0.11)
$\varepsilon_{1\infty}$	0.0	0.2	0.2	0.2	0.2	0.2	0.2	0.2
			(0.2)	(0.2)	(0.2)	(0.2)	(0.2)	(0.2)
d(Å)	—	—	4386	4372	4370	4370	4359	4352
			(14)	(28)	(30)	(30)	(41)	(48)
σ	—	—	0.0086	0.0084	0.0080	0.0090	0.0098	0.0128

Fig. 5, the $\varepsilon(E)$ spectra for the annealed samples clearly differ from that of the as-implanted, fully amorphous sample (t=0 s).

We show in Fig. 6 the SE $\varepsilon(E)$ spectra for N^+ ion-implanted and annealed samples at 750 °C for t=40, 60, and 80 s. The solid lines are obtained by solving the four-phase model (substrate/damaged layers 1 and 2/ambient) as shown at the top of Fig. 6. Here, the annealed samples are assumed to have discrete homogeneous μc-Si layers with different degree of microcrystallinity. It is expected that the longer the annealing time, the larger the microcrystallinity size in the damaged layer. The $\varepsilon(E)$ spectra for μc-Si are deduced by solving the Fresnel's formula. The corresponding MDF parameters are given in Table II. The damaged layer thicknesses d_1 and d_2 and the LRA parameter σ obtained here are also listed in Table II.

The μc-Si $\varepsilon(E)$ spectra deduced here differ appreciably from that of c-Si, especially in the vicinity of the CP's (see Fig. 11 in the Appendix). As an example, we show in Fig. 6(c) by the dashed lines the simulated results assuming c-Si instead of μc-Si. It is understood that the assumption of c-Si provides no good agreement with the experimental data, especially in the vicinity of the E_1 (~3.4 eV) and E_2 (~5.2 eV) structures.

A large number of studies have been performed to understand an amorphization mechanism due to ion implantation into semiconductors.[28] Two competing models are proposed for this purpose: (i) heterogeneous and (ii) homogeneous amorphization models. In the heterogeneous model, amorphization is assumed to occur initially in the cylindrical region around each ion path.[29] The continuous amorphous layer is formed due to sufficient overlap of the

Downloaded 11 Oct 2007 to 210.151.113.98. Redistribution subject to AIP license or copyright, see http://jap.aip.org/jap/copyright.jsp

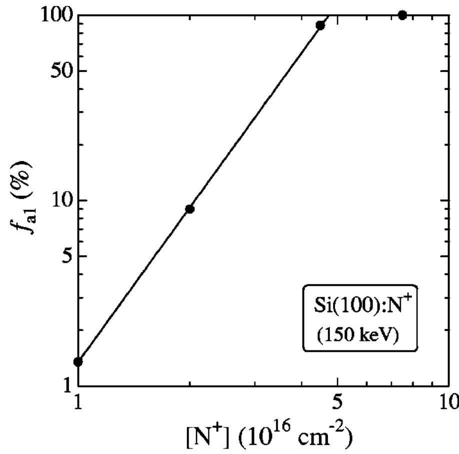

FIG. 4. Amorphous fraction f_{a1} (Layer 1), obtained from the four-phase model, as a function of ion fluence $[N^+]$. The solid line represents the calculated result of Eq. (8).

amorphized cylindrical regions. In the homogeneous model, on the other hand, amorphization is supposed to be a phase transition induced by the accumulation of damage, above a certain threshold, resulting from the passage of energetic ions.[30,31]

As demonstrated in Fig. 3, not only the crystalline but also the amorphous $\varepsilon(E)$ spectra can be modeled by the common MDF expressions over the entire range of photon energies. The MDF requires three fitting parameters, the CP energy, the strength parameter, and the lifetime broadening, at each CP. The key finding to achieve good agreement between the calculated and the experimental spectra for *a*-Si is the use of the different CP parameters from the crystalline ones. By monitoring the CP parameters, thus, we can conclude whether an ion-implanted material is still in the crystalline state or not[32] or, similarly, whether an ion-implanted and subsequently annealed sample is still in the amorphous state or not.[33] If a turning point in the CP parameter vs ion fluence or annealing time plot is observed, it may indicate the onset of crystalline/amorphous phase transition.

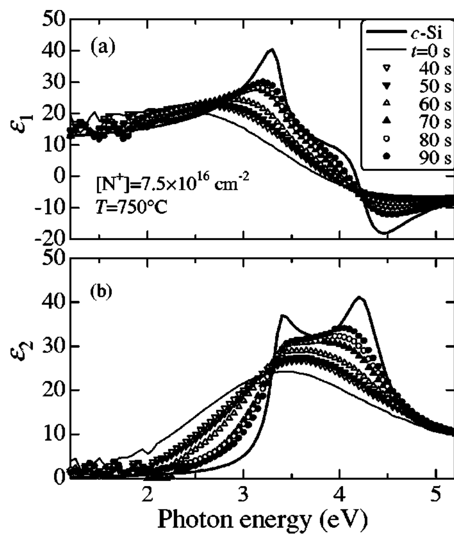

FIG. 5. Dielectric-function spectra, $\varepsilon(E)=\varepsilon_1(E)+i\varepsilon_2(E)$, for N^+ ion-implanted Si(100) at 150 keV with a dose of 7.5×10^{16} cm^{-2}. The samples were annealed at 750 °C for six different times, t=40, 50, 60, 70, 80, and 90 s. For comparison, the $\varepsilon(E)$ spectra for unimplanted (*c*-Si) and as-implanted samples (t=0 s) are shown by the heavy and the light solid lines, respectively.

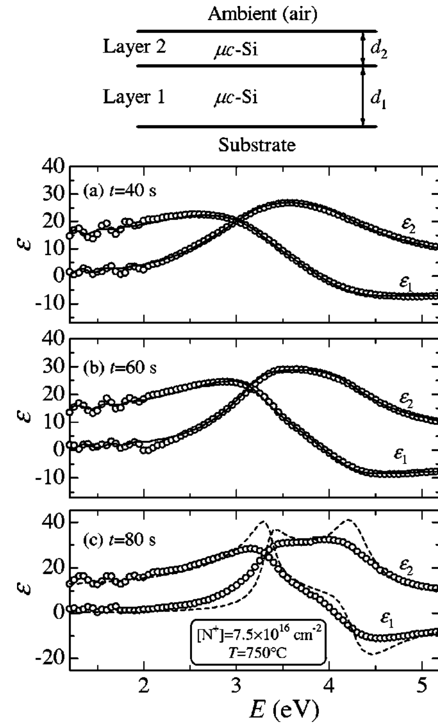

FIG. 6. $\varepsilon(E)$ spectra for N^+ ion-implanted (7.5×10^{16} cm^{-2}) and annealed samples at 750 °C for t=40, 60, and 80 s. The open circles show the experimental data. The solid lines represent the calculated results using the four-phase (substrate/μc-Si/μc-Si/ambient) model as depicted before this figure. The MDF parameters for μc-Si obtained in this analysis are summarized in Table II. The damaged layer thicknesses d_1 and d_2 and unbiased estimator σ are also listed in the last two rows in Table II.

Figure 7 plots the CP energies, E_1, E_2, E_0', and E_1', as a function of annealing time t for N^+ ion-implanted Si(100) samples. We can see in Fig. 7 a gradual increase in E_g's and their turning point at $t\sim70$ s.

The difference in the electronic properties between *c*-Si and *a*-Si has been discussed in detail by Thorpe and Weaire[34] and by Joannopoulos and Cohen.[35,36] It has been shown that the lower-energy shifts in the density-of-states peaks observed in amorphous materials are related to the variations in the tetrahedral bond angles, which are known to exist even in

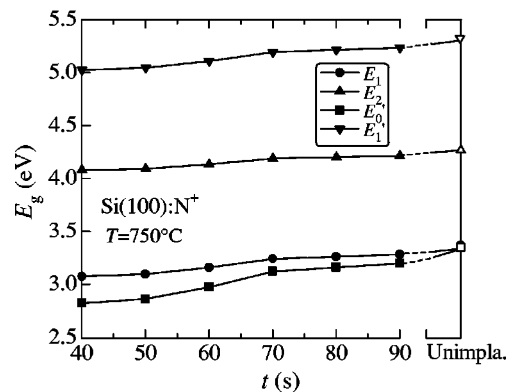

FIG. 7. Plots of the E_1, E_2, E_0', and E_1' CP energies as a function of annealing time t at 750°C for N^+ ion-implanted Si(100) samples (7.5×10^{16} cm^{-2}).

Downloaded 11 Oct 2007 to 210.151.113.98. Redistribution subject to AIP license or copyright, see http://jap.aip.org/jap/copyright.jsp

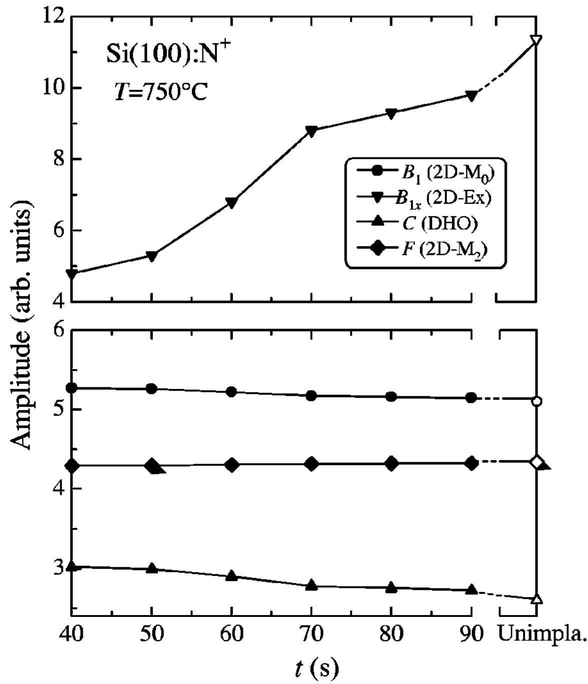

FIG. 8. Plots of the strength parameters for some prominent interband transitions; B_1 (E_1,2D-M_0 CP); B_{1x} (E_1, 2D exciton); C (E_2, DHO); and F (E_2,2D-M_2 CP); as a function of annealing time t at 750 °C for N^+ ion-implanted Si(100) samples (7.5×10^{16} cm^{-2}).

the amorphous phase. Such shifts in the density-of-states peaks may also be the cause for the lower shifts in the interband transition energies in amorphous substances.[25]

Figure 8 shows the strength parameters for some important interband transitions; B_1 [E_1, two-dimensional (2D) M_0 CP]; B_{1x} [E_1, 2D exciton]; C [E_2, damped harmonic oscillator (DHO)]; and F [E_2, 2D-M_2 CP], vs annealing time t for N^+ ion-implanted Si(100) samples. As in Fig. 7 (E_g's), the strength parameters suggest the presence of their turning point at $t\sim70$ s. It is also seen that the strength parameters B_1 and C decrease, while B_{1x} and F increase, with increasing t. At present, unfortunately, we cannot give a complete interpretation for this dependence.

The broadening parameters for some important interband transitions; Γ (E_1,2D-M_0 CP and 2D exciton); γ (E_2, DHO); and Γ (E_2,2D-M_2 CP), are plotted in Fig. 9 as a function of annealing time t. These parameters change dramatically at t below and above ~70 s. It is also interesting to point out that amorphous materials preserve the short-range order, in the present case the tetrahedral coordination, but do not preserve the long-range order. It is, therefore, natural to consider that the larger broadenings required in the shorter-time annealed sample is mainly due to the effects of the long-range disorder and the short-range defects (i.e., a change in the tetrahedral bond lengths and/or angles). A decrease in Γ and γ in Fig. 9 for $t\geqslant70$ s is, thus, thought to be due to restoration of such structural defects.

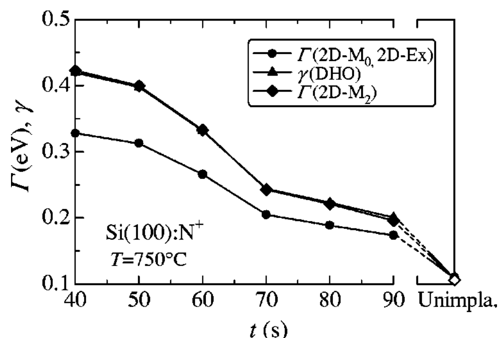

FIG. 9. Plots of the broadening parameters for some of the important interband transitions; Γ (E_1,2D-M_0 CP and 2D exciton); γ (E_2, DHO); and Γ (E_2,2D-M_2 CP); as a function of annealing time t at 750 °C for N^+ ion-implanted Si(100) samples (7.5×10^{16} cm^{-2}).

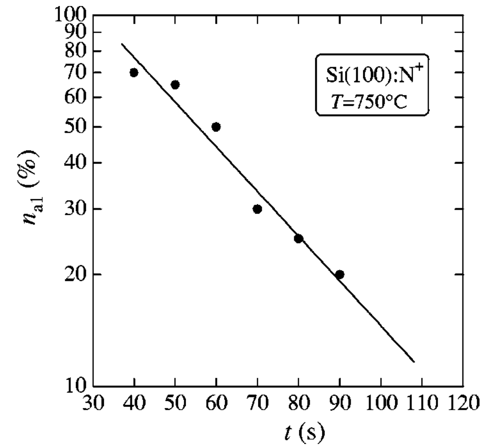

FIG. 10. Plots of the percentage of amorphousness η_{a1} (Layer 1), defined by Eq. (9), as a function of annealing time t at 750 °C. The solid line represents the calculated result of Eq. (10).

Regarding that the perfect crystalline and the fully amorphous states are extremes in the parameter describing the percentage of amorphousness, η_a, with 0% and 100%, respectively, let us define η_a for μc-Si by

$$\eta_a(\%) = \frac{E_1(c\text{-Si}) - E_1(\mu c\text{-Si})}{E_1(c\text{-Si}) - E_1(a\text{-Si})} \times 100, \quad (9)$$

where E_1 is the E_1 CP energy for c-Si (3.37 eV), a-Si (2.95 eV), or μc-Si.

Figure 10 plots the percentage of amorphousness η_{a1} in Layer 1 as a function of annealing time t for samples annealed at 750 °C. From these plots, we obtain that η_{a1} decreases with increasing annealing time t as

$$\eta_{a1} = 2.34 \exp\left(-\frac{t}{t_0}\right), \quad (10)$$

where t_0 is the time constant for defect annealing. The solid line in Fig. 10 represents the calculated result of Eq. (10).

The time constant t_0 for N^+ ion-implanted Si(100) annealed at 750 °C is determined to be 36 s. We can, however, give no detailed discussion on the validity of this value. This is because there have been reported no similar data in the literature. We note, however, that the time constant is one of the most essential parameters in various rapid thermal processing, such as rapid thermal annealing, crystallization, oxidation, nitridation, and deposition.

V. CONCLUSIONS

The SE was used to characterize N^+ ion-implanted and rapid thermally annealed Si(100) wafers. The N^+ ion implan-

Downloaded 11 Oct 2007 to 210.151.113.98. Redistribution subject to AIP license or copyright, see http://jap.aip.org/jap/copyright.jsp

tation was performed at 150 keV with fluences from 1×10^{16} to 7.5×10^{15} cm^{-2} at room temperature. The as-implanted Si(100) surfaces were subdivided into two layers, each consisting of volume fractions of crystalline and amorphous silicon. The resulting four-phase model gave an excellent agreement with the experimental data. The rapid thermal annealing was carried out at 750 °C between 40 and 90 s in a dry N_2 atmosphere. The $\varepsilon(E)$ spectra taken after annealing were reasonably interpreted by the MDF with properly changing the CP parameters. The fit-determined CP parameters showed a distinct transition from the amorphous to crystalline state for $t \sim 70$ s. The time constant for defect annealing was also determined to be $t_0=36$ s. The SE has thus been proven to be an easy, fast, and nondestructive technique that can be used to assess important ion-implantation process parameters.

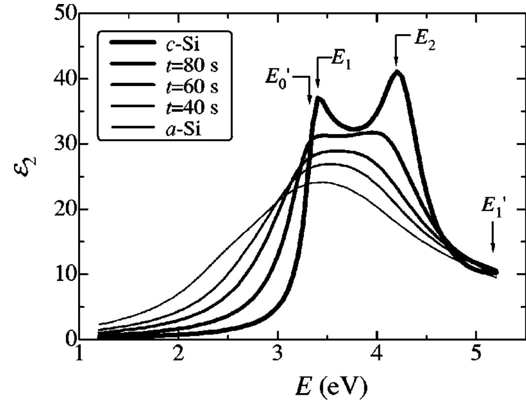

FIG. 11. Imaginary part of the dielectric function $\varepsilon_2(E)$ for μc-Si deduced from the four-phase model, together with those for perfectly crystalline (c-Si) and as-implanted, fully amorphous silicon (a-Si). The μc-Si $\varepsilon_2(E)$ spectra correspond to those annealed at 750 °C for $t=40, 60$, and 80 s (Layer 1).

ACKNOWLEDGMENTS

The authors are indebted to Dr. T. Miyazaki and Dr. S. Ozaki for their kind advice concerning this work.

APPENDIX: MODEL DIELECTRIC FUNCTION

In the following, we briefly summarize the MDF for the CP's of each energy gap (E_1, E_2, E_0', and E_1') in tetrahedrally bonded semiconductors.[24,25] Combining all these contributions, the spectral dependence of $\varepsilon(E)$ can be obtained for both crystalline and amorphous semiconductors.

The E_1 CP may be of the 2D M_0 type and occur in silicon at energies around ~3.4 eV. The contribution to $\varepsilon(E)$ of this type of CP is given by

$$\varepsilon(E) = -B_1 \chi_1^{-2} \ln(1-\chi_1^2), \tag{A1}$$

with

$$\chi_1 = \frac{E+i\Gamma}{E_1}, \tag{A2}$$

where B_1 and Γ are, respectively, the strength and the broadening parameters of the E_1 transitions.

The contribution of the 2D-M_0 excitonic transitions to $\varepsilon(E)$ is written, with a Lorentzian line shape, as

$$\varepsilon(E) = \sum_{n=1}^{\infty} \frac{B_{1x}}{(2n-1)^3} \times \left[\frac{1}{(E_1 - [4G/(2n-1)^2])^2 - E^2 - i2E\Gamma} \right], \tag{A3}$$

where B_{1x} is the exciton strength parameter and G is the 2D exciton Rydberg energy. We have made the assumption $G = 0$ eV, since the detailed value is not yet well known for silicon.

The E_2 transitions in silicon occur at ~4.3 eV. The nature of these transitions is more complicated, because it does not correspond to a single, well-defined CP. Here we characterize these transitions by a mixture of DHO and 2D maximum (2D-M_2 CP). The DHO can now be written as

$$\varepsilon(E) = \frac{C}{(1-\chi_2^2) - i\chi_2\gamma}, \tag{A4}$$

with

$$\chi_2 = \frac{E}{E_2}, \tag{A5}$$

where C and γ are, respectively, the nondimensional strength and the broadening parameters of the DHO.

The contribution of the 2D-M_2 CP to $\varepsilon(E)$ can be written as

$$\varepsilon(E) = -F\chi_{2m}^{-2} \ln \frac{1-\chi_{cl}^2}{1-\chi_{2m}^2}, \tag{A6}$$

with

$$\chi_{2m} = \frac{E+i\Gamma}{E_2}, \tag{A7}$$

$$\chi_{cl} = \frac{E+i\Gamma}{E_{cl}}. \tag{A8}$$

In Eqs. (A6)–(A8), F and Γ are the strength and the broadening parameters of the 2D-$M_2(E_2)$ transitions, respectively, and E_{cl} is a low-energy cutoff assumed to occur at E_1.

The E_0' transitions (~3.35 eV) in silicon are believed to occur at Γ or in the Δ direction near the Γ point. The E_1' transitions (~5.3 eV) are also expected to occur at or near the L point. These CP's are not so strong, and hence, they are simply characterized by the DHO.

The $E_0/(E_0+\Delta_0)$ structures in silicon appear in the spectrum between the dominant E_1 and E_2 structures. As a result, its exceedingly weak nature would be completely overshadowed by them. Because of this, we shall not take into account the contribution of these transitions in the $\varepsilon(E)$ spectra.

The $\varepsilon(E)$ spectra for c-Si, μc-Si, and a-Si can be calculated from the sum of Eqs. (A1), (A3), (A4), and (A6) [$\varepsilon_1(E) = \text{Re}\ \varepsilon(E); \varepsilon_2(E) = \text{Im}\ \varepsilon(E)$]. It should be noted, however, that the experimental ε_1 values are usually somewhat larger than those obtained from the MDF calculation. To im-

Downloaded 11 Oct 2007 to 210.151.113.98. Redistribution subject to AIP license or copyright, see http://jap.aip.org/jap/copyright.jsp

prove the fit, therefore, we included in the calculation an additional term, $\varepsilon_{1\infty}$, in ε_1. This constant term may arise from other higher-lying interband transitions.

We compare in Fig. 11 the $\varepsilon_2(E)$ spectra for μc-Si with those for unimplanted, perfectly crystalline (c-Si) and as-implanted, fully amorphous silicon (a-Si). The μc-Si $\varepsilon_2(E)$ spectra were taken after annealing at 750 °C for t=40, 60, and 80 s (Layer 1). The corresponding CP parameters are summarized in Table II. It is found that the μc-Si $\varepsilon(E)$ spectra are strongly dependent on annealing time t. In particular, the longer the annealing time, the stronger E_2 is. It is also noted that the μc-Si spectra in Fig. 11 resemble those reported in the literature.[37–39]

[1] K. Sumino, I. Yonenaga, M. Imai, and T. Abe, J. Appl. Phys. **54**, 5016 (1983).
[2] R. J. Dexter, S. B. Watelski, and S. T. Picraux, Appl. Phys. Lett. **23**, 455 (1973).
[3] M. Fried, T. Lohner, J. M. M. de Nijs, A. van Silfhout, L. J. Hanekamp, Z. Laczik, N. Q. Khanh, and J. Gyulai, J. Appl. Phys. **66**, 5052 (1989).
[4] D. E. Davies, J. A. Adamski, and E. F. Kennedy, Appl. Phys. Lett. **48**, 347 (1986).
[5] J. M. Poate and J. S. Williams, *Ion Implantation and Beam Processing*, edited by J. S. Williams and J. M. Poate (Academic, New York, 1984), p. 13.
[6] B. Drosd and J. Washburn, J. Appl. Phys. **51**, 4106 (1980).
[7] R. E. Hummel, W. Xi, and D. R. Hagmann, J. Electrochem. Soc. **137**, 3583 (1990).
[8] P. K. Giri, S. T. Sundari, G. Raghavan, B. K. Panigrahi, P. Magudapathy, K. G. M. Nair, and A. K. Tyagi, J. Appl. Phys. **90**, 659 (2001).
[9] S. T. Sundari, J. Appl. Phys. **92**, 4367 (2002).
[10] V. P. Popov, I. V. Antonova, A. K. Gutakovsky, E. V. Spesivtsev, and I. I. Morosov, Mater. Sci. Eng., B **73**, 120 (2000).
[11] W. Fukarek and J. R. Kaschny, J. Appl. Phys. **86**, 4160 (1999).
[12] S. Lee, S. Y. Kim, and S. Oh, Jpn. J. Appl. Phys., Part 1 **35**, 5929 (1996).
[13] N. V. Nguyen and K. Vedam, J. Appl. Phys. **67**, 3555 (1990).
[14] T. M. Burns, S. Chongsawangvirod, J. W. Andrews, E. A. Irene, G. McGuire, and S. Chevacharoeukul, J. Vac. Sci. Technol. B **9**, 41 (1991).
[15] M. Fried, T. Lohner, W. A. M. Aarnink, L. J. Hanekamp, and A. van Silfhout, J. Appl. Phys. **71**, 5260 (1992).
[16] H. Mori, S. Adachi, and M. Takahashi, J. Appl. Phys. **90**, 87 (2001).
[17] K. Tsunoda, S. Adachi, and M. Takahashi, J. Appl. Phys. **91**, 2936 (2002).
[18] P. Petrik, O. Polgár, M. Fried, T. Lohner, N. Q. Khánh, and J. Gyulai, J. Appl. Phys. **93**, 1987 (2003).
[19] M. Fried, T. Lohner, W. A. M. Aarnink, L. J. Hanekamp, and A. van Silfhout, J. Appl. Phys. **71**, 2835 (1992).
[20] X.-F. He, R.-R. Jiang, R.-X. Chen, and D. Mo, J. Appl. Phys. **66**, 5261 (1989).
[21] S. Adachi, T. Matsumura, and T. Suzuki, Jpn. J. Appl. Phys., Part 1 **33**, 1931 (1994).
[22] M. Erman, J. B. Theeten, P. Chambon, S. M. Kelso, and D. E. Aspnes, J. Appl. Phys. **56**, 2664 (1984).
[23] R. M. A. Azzam and N. M. Bashara, *Ellipsometry and Polarized Light* (North-Holland, Amsterdam, 1977).
[24] S. Adachi, *Optical Properties of Crystalline and Amorphous Semiconductors: Materials and Fundamental Principles* (Kluwer Academic, Boston, 1999).
[25] S. Adachi, H. Mori, and S. Ozaki, Phys. Rev. B **66**, 153201 (2002).
[26] P. Lautenschlager, M. Garriga, L. Vina, and M. Cardona, Phys. Rev. B **36**, 4821 (1987).
[27] S. Adachi, Phys. Rev. B **38**, 12966 (1988).
[28] S. U. Campisano, S. Coffa, V. Raineri, F. Priolo, and E. Rimini, Nucl. Instrum. Methods Phys. Res. B **80/81**, 514 (1993).
[29] F. F. Morehead, Jr. and B. L. Crowder, Radiat. Eff. **6**, 27 (1970).
[30] M. L. Swanson, J. R. Parsons, and C. W. Hoelke, Radiat. Eff. **9**, 249 (1971).
[31] O. W. Holland, S. J. Pennycook, and G. L. Albert, Appl. Phys. Lett. **55**, 2503 (1989).
[32] S. Adachi, H. Mori, and M. Takahashi, J. Appl. Phys. **93**, 115 (2003).
[33] S. Hikino and S. Adachi, J. Phys. D **37**, 1617 (2004).
[34] M. F. Thorpe and D. Weaire, Phys. Rev. Lett. **27**, 1581 (1971).
[35] J. D. Joannopoulos and M. L. Cohen, Phys. Rev. B **7**, 2644 (1973).
[36] J. D. Joannopoulos and M. L. Cohen, Phys. Rev. B **8**, 2733 (1973).
[37] H. Touir and P. Roca i Cabarrocas, Phys. Rev. B **65**, 155330 (2002).
[38] K. H. Jun, R. Carius, and H. Stiebig, Phys. Rev. B **66**, 115301 (2002).
[39] T. D. Kang, H. Lee, S. J. Park, J. Jang, and S. Lee, J. Appl. Phys. **92**, 2467 (2002).

Downloaded 11 Oct 2007 to 210.151.113.98. Redistribution subject to AIP license or copyright, see http://jap.aip.org/jap/copyright.jsp